STUDY ON URBAN HEAT ISLAND OF BEIJING USING ASTER DATA ----A QUANTATIVE REMOTE SENSING PERSPECTIVE

Yan Binyan, Fan Wenjie, TaoXin, XuXiru

Institute of Remote Sensing and Geographic Information System, Peking University
Email Address: fanwj@pku.edu.cn (Fan Wenjie)

ABSTRACT

The urban heat island (UHI) becomes a very serious problem in China. In this paper, the UHI pattern of Beijing in the four seasons was studied using ASTER thermal infra-red data. The Land Surface Temperature(LST) maps of Beijing, China in the four seasons of 2004 were retrieved using local split window algorithm adjusted according to ASTER data and the atmosphere profiles of Beijing. And a numerical simulation showed the reliability of the retrieval results. It is found that LST in urban and rural areas display evident differences. The differences varied with seasons, and UHI is the most intensive in summer, with the intensity of around 0.6~1.5K, which is better explained by vegetation coverage differences in four seasons. Patterns of LST distribution were found to be closely related to land use types and seasons.

Index Terms— Remote sensing

1. INTRODUCTION

Since the rapid development of urbanization, the urban heat island (UHI) becomes a more and more serious problem. Many studies [1, 2] have employed thermal remote sensing to examine the intensity and the spatial pattern of UHI and its relation to land surface characteristics since Rao[3]. UHI can be studied on regional scale by remote sensing technology which is much better than traditional method based on ground observations. LST (Land Surface Temperature) is one of the most important parameters of UHI study, and it has been used to analyze UHI in many cases [4, 5]. ASTER (Advanced Space borne Thermal Emission and Reflection Radiometer) data are suitable for LST retrieval because of its high resolution in both spectrum and space dimension [6], so that the mixed pixel problem can be released and high resolution of LST can be gained. The aim of this paper is to analyze the UHI patterns of Beijing and its seasonal variety by means of LST retrieval using ASTER data. Beijing is a representative metropolis with rapid development of urbanization, so the results and analytical methods of this paper are also applicable to other big cities.

2. METHODOLOGY

2.1. Study Area

The city of Beijing is located in the North of China. The mountains elevated from 1km to 1.5 km distribute in the west, north and east-north sides and a plain with an elevation ranges from 20m to 60m locate in the south-east side sloping to the Bohai Sea. Beijing covers an area of 16, 800 km² with a population of 11, 540, 000, while the urban region covers12, 358 km² with a population of 10,360,000. Beijing is now experiencing the rapid economic development.

2.2. Image Processing

ASTER can offer fourteen channels with three different spatial resolutions, 15m(visible and near infra-red bands), 30m(short wave infra-red bands), and 90m(thermal infra-red bands). It has 5 thermal infra-red bands, which are 8.125-8.475μm, 8.475-8.825μm, 8.925-9.275μm, 10.25-10.95μm and 10.95-11.65μm.

Five ASTER images of level 1B on Apr.9, Jun.12, Oct.18 and Jan.27, 2004 respectively are utilized, which cover the urban and the surrounding rural areas of Beijing. The images were geometrically corrected and calibrated.

2.3. LST Retrieval

The radiance received by the sensor in thermal infra-red bands is expressed as

$$L_\lambda(\theta) = t_{\lambda 0}\varepsilon_\lambda(\theta)L_{b\lambda}(T_s) + t_{\lambda 0}\int_{2\pi} f_t(\theta'-\theta)L^{\downarrow}{}_{a\lambda}(\theta')\cos\theta' d\Omega' + L^{\uparrow}{}_{a\lambda}(\theta) \quad (1),$$

LST is retrieved using local split window algorithm as a linear equation of the brightness temperatures of band 13 and 14 (10.25-10.95μm, 10.95-11.65μm respectively) [7]. So LST T_s is calculated as

$$T_s = \frac{T_{s1}+T_{s2}}{2} + \frac{T_{s1}-T_{s2}}{2}\cdot\frac{D_1+D_2}{D_1-D_2} - \beta W\frac{A_1A_2}{D_1-D_2}[L_1\gamma_1\frac{1-\varepsilon_1}{\varepsilon_1} - L_2\gamma_2\frac{1-\varepsilon_2}{\varepsilon_2}] \quad (2),$$

where T_{s1} and T_{s2} are the brightness temperatures of the two thermal bands. β is related to the sensor viewing angle and γ_i (i=1,2) is a function of emissivity, which can both be calculated easily. But since split window algorithm was first introduced for AVHRR data [8], the experiential coefficients namely D_1 , D_2 , W, A_1 and A_2 , should be adjusted according to atmospheric conditions of Beijing, for the use of ASTER data. In this work, these coefficients are obtained using Look Up Table method with the aid of MODTRAN 4.0 software package, the ASTER response functions of band 13 and 14 and 393 standard atmospheric profiles in the north hemisphere of TIGR database. Let X stand for $\frac{D_1 + D_2}{D_1 - D_2}$ and Y for $W\frac{A_1 A_2}{D_1 - D_2}$ in term (2), the values of them are listed in Table 1.

Table 1 values of parameters applicable to ASTER

seasons	para-meter	water	vegetation	soil	concrete
spring	X	8.693	9.348	7.284	9.421
	Y	2.440	3.165	-2.315	8.870
summer	X	9.867	9.900	9.822	9.961
	Y	1.215	0.373	-0.126	1.145
autumn	X	10.302	15.006	6.613	15.168
	Y	0.830	0.668	-0.243	2.046
winter	X	11.648	2.401	12.534	12.473
	Y	0.648	3.465	-2.696	6.344

The emissivity values are obtained from an emissivity map generated from VNIR bands (band1, band2 and band3). Before resampled to the same spatial resolution (90 m) with TIR images, the VNIR images were classified into four land use types, namely water body, vegetation, bare soil and concrete. And then emissivity values obtained from ASTER Spectral Library (Table 2) are assigned to different land use types and different bands to produce an emissivity map.

Table 2 emissivity values of bands 13 and 14

	water	vegetation	soil	concrete
band 13	0.992789	0.951653	0.953828	0.966658
band 14	0.991897	0.950955	0.96631	0.967098

3. RESULTS AND ANALYSIS

3.1 LST Distribution

The LST distribution maps in the four seasons are shown in Graph 1. The same geographic region is selected by the green lines in the four images. The three circles in each image from inside to outside are the second, the fourth and the fifth ring road respectively, which features the level of urban spread to some extent.

3.2 Errors

Lacking of in-situ measurements, a numerical simulation is used to assess the accuracy of LST retrieved. A certain percentage of Gaussian distributed noises are added to 100 randomly generated LST which ranges from -2.8K to 1.9K with the standard deviation of 0.995K. MORTRAN 4.0 is used to calculate the radiances received by the sensor from the LST with noises added and then the radiance calculated is transformed to LST using the local split window algorithm. Errors are calculated and the standard deviation is listed in Table 3. Noises are not amplified, showing the retrieval results in section 3.1 are credible.

Table 3 Errors

Percentage of noises added	5%	10%	20%	50%	100%
Standard deviation	0.4692	0.4740	0.5045	0.6708	1.1051

3.3 Analysis

The histograms of LST distribution in the four seasons are presented in Figure 2. And the statistics including the minimum LST, the maximum LST, the mean LST, the mode of LST and the standard deviation of LST of both the urban areas and the rural areas are calculated, and the test statistics are also derived to examine the difference of LST between the two regions (see Table 4).

Urban areas and rural areas exhibit evident difference in LST at 0.005 confidence level. Rural area displays a cooler LST compared with urban area in summer and autumn, which is the reverse in spring and winter. Urban heat island effect exists in summer and autumn and is the most intensive in summer. The intensity of urban heat island in summer is around 0.6~1.5K. It is found that the above results are better explained by differences of vegetation coverage between urban and rural area in the four seasons(Table 5). The differences of vegetation coverage are larger in summer and autumn when urban heat island effect exists. In spring and winter, the differences are not evident.

According to the analysis based on the statistical data obtained, patterns of LST distribution are found to be closely related to land use types and seasons. Higher LST is observed in the bare soil and the concrete and lower one in the water body and the vegetation. The differences between LST of different land use types are larger in warm seasons.

Table 5 vegetation coverage in urban and rural areas

	spring	summer	autumn	winter
vegetation coverage in urban area(%)	22.49	13.27	16.81	8.60
vegetation coverage in rural area(%)	30.05	30.37	34.41	10.59

4. CONCLUSION

(1) The parameters in local split window algorithm were adjusted according to atmospheric conditions of Beijing in order to apply ASTER data using Look Up Table method with the aid of MODTRAN 4.0 software package, the ASTER response functions of band 13 and 14 and standard atmospheric profiles of TIGR database;
(2) Urban Heat Island is the most intensive in summer, with the intensity of 0.6~1.5K; the LST distribution patterns are found to be closely related to land use types and seasons;
(3) The UHI is affected by various factors, such as the wind speed and the air temperature, the seasonal variety deserves further study using more data, and this paper is just an attempt.

5. REFERENCES

[1] Roth, M., T.R. Oke, W.J. Emery, "Satellite-derived urban heat islands from three coastal cities and the utilization of such data in urban climatology", INT.J.REMOTE SENSING, vol. 10, no. 11, pp.1699–1720, 1989.

[2] Carlson, T.N., J.A. Augustine, F.E. Boland, "Potential Application of Satellite Temperature Measurements in the Analysis of Land Use over Urban Areas", Bulletin of the American Meteorological Society, vol. 58, no. 12, pp. 1301–1303,1977.

[3] Rao, P.K., "Remote sensing of urban 'heat islands' from an environmental satellite", Bulletin of the American Meteorological Society, vol. 53, no. 7, pp. 647–648, 1972.

[4] Gupta, R. K., S. Prasad., M. V. R. Sesha Sai, et al., "The estimation of surface temperature over an agricultural area in the state of Haryana and Panjab, India, and its relationship with the Normalized Difference Vegetation Index (NDVI), using NOAA–AVHRR data", INT. J.REMOTE SENSING, vol. 18, no. 18, pp. 3729–3741, 1997.

[5] Streutker, D. R., "Satellite-measured growth of the urban heat island of Houston, Texas", Remote Sensing of Environment, vol. 85, pp. 282-289, 2003.

[6] M. Abrams, S. Hook, ASTER User Handbook, Jet Propulsion Laboratory/California Institute of Technology.

[7] F. Becker, Z.L. Li, "Towards a local split window method over land surfaces", INT.J.REMOTE SENSING, vol.11, no.3, pp. 369–393, 1990.

[8] Dash, P., Gottsche, F. M., Olesen, F. S., et al., "Land surface temperature and emissivity estimation from passive sensor data: Theory and practice-current trends", INT. J.REMOTE SENSING, vol.23, no.13, pp. 2563–2594, 2002.

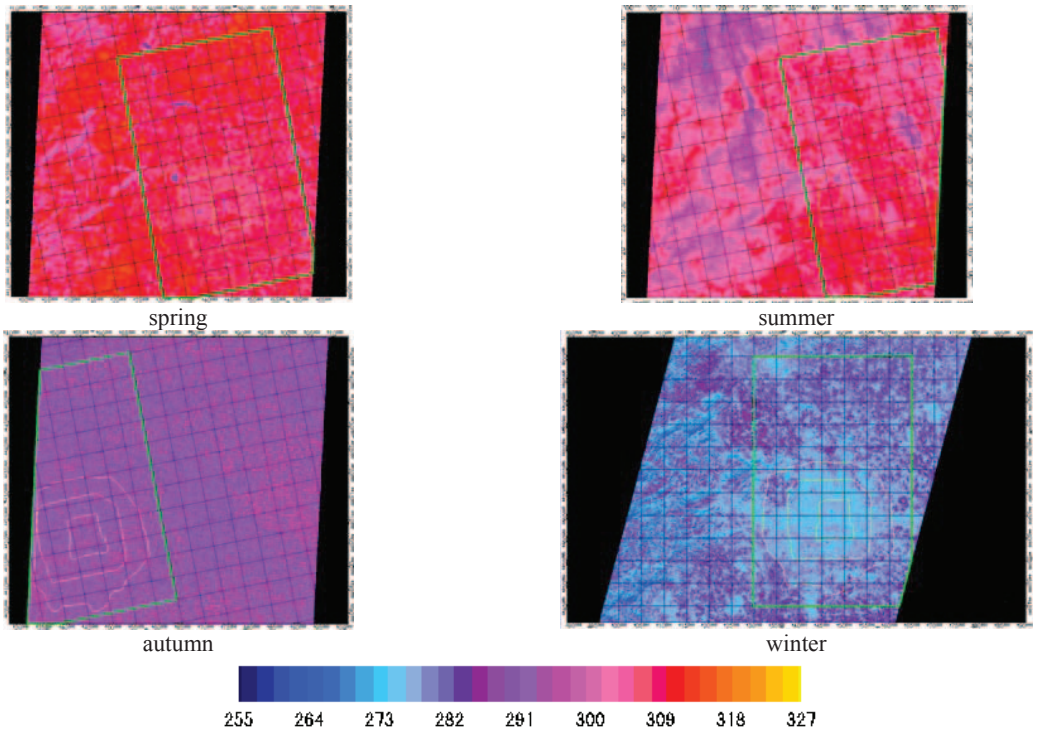

Figure1 LST distribution maps

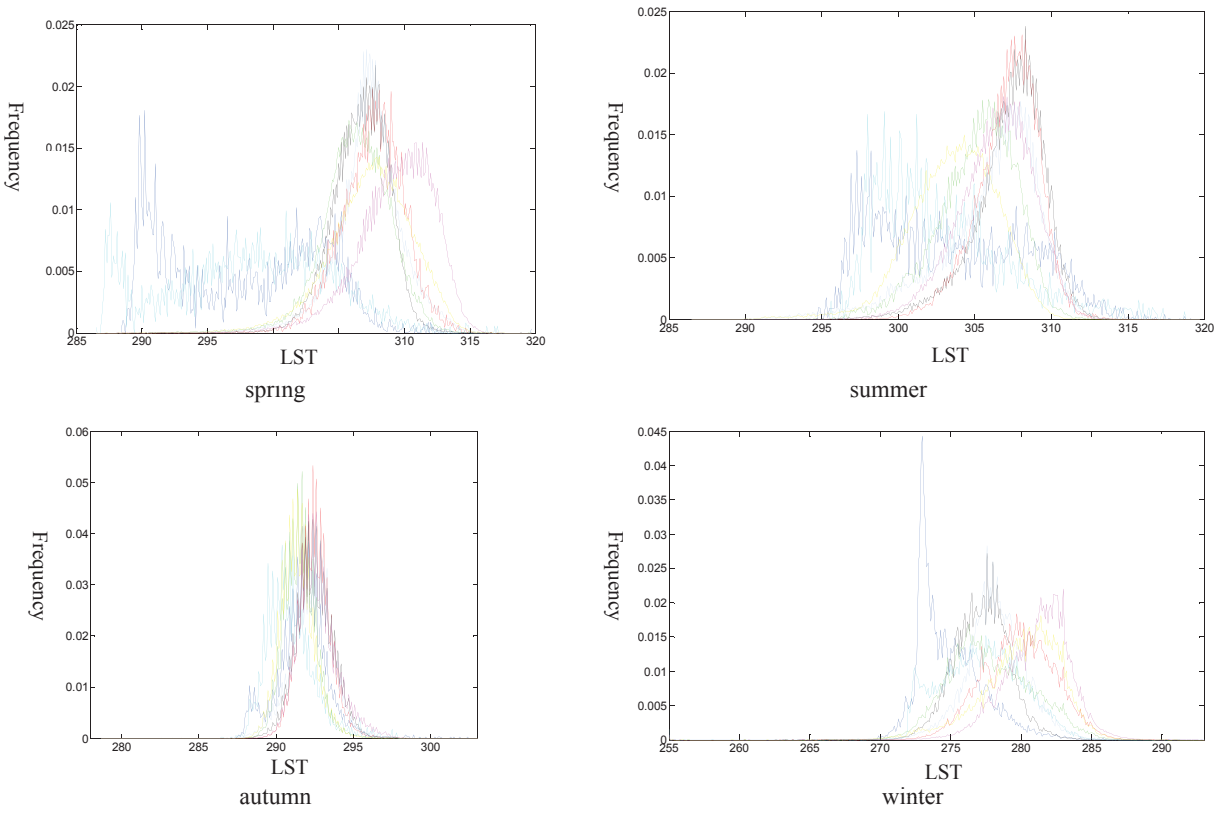

Figure 2 the histograms of LST distribution in the four seasons

Table 4 statistics of LST in urban and rural areas

seasons	land use types	maximum		minimum		mean		mode		standard deviation		test statistics
		urban area	rural area	urban area	rural area	urban area	rural area	urban area	rural area	urban area	rural area	
spring	water	319.7	317.1	288.5	286.5	298.0	298.2	290.2	287.6	5.877	6.073	4.945
	vegetation	319.7	317.6	290.3	287.3	306.3	307.4	305.8	308.1	2.609	3.157	263.1
	soil	316.6	317.4	291.5	288.1	307.6	309.4	307.6	311.4	2.395	2.950	259.7
	concrete	319.7	317.5	289.9	287.2	306.7	307.3	307.8	307.1	2.146	2.627	254.5
summer	water	319.6	318.7	294.8	293.3	303.5	302.9	297.3	299.1	4.831	4.237	18.77
	vegetation	314.3	314.4	292.8	288.8	305.1	303.6	305.9	304.3	2.580	2.883	304.5
	soil	314.9	314.7	291.7	290.3	307.2	306.4	308.1	306.9	2.047	2.460	186.8
	concrete	316.9	314.8	290.1	288.8	307.3	305.9	308.3	308.0	2.350	3.451	414.9
autumn	water	302.4	299.3	278.7	286.4	291.7	291.0	291.7	290.9	1.643	1.543	67.01
	vegetation	299.6	298.9	287.4	287.1	291.6	291.4	291.7	291.4	1.066	1.101	95.42
	soil	299.6	298.6	283.9	286.4	292.5	292.7	292.4	292.6	1.049	1.308	83.90
	concrete	302.4	300.7	278.7	285.7	292.5	292.3	292.4	292.6	1.233	1.385	121.4
winter	water	290.9	293.0	266.2	255.0	275.0	277.3	273.3	278.3	2.361	2.903	122.5
	vegetation	292.9	293.0	265.5	255.0	280.2	282.4	279.1	284.0	3.040	2.954	318.5
	soil	292.9	293.0	264.8	255.0	282.6	284.0	284.5	284.5	2.659	2.541	363.6
	concrete	292.9	293.0	262.1	255.0	279.4	280.3	279.9	279.9	2.346	2.538	399.8